Proceedings of the Twenty-third (2013) International Offshore and Polar Engineering **www.isope.org**
Anchorage, Alaska, USA, June 30–July 5, 2013

ISBN 978-1-880653-99–9 (Set); ISSN 1098-6189 (Set)

Predicting powering performance changes for ships in offshore conditions from small design modifications

Björn Windén[1], *Stephen Turnock*[1] *and Dominic Hudson*[1]
[1]Fluid Structure Interactions Research Group University of Southampton
Southampton, United Kingdom.

ABSTRACT

This paper addresses the prediction of ship performance in waves by means of RANS-based CFD. Lately, much attention has been given to modelling the complex geometry (moving hull and rotating propeller) which can sometimes distort or suppress the importance of the underlying physics. The approach here is to subject a fixed hull to waves and study how the flow around the hull is affected and what this means for the inflow to the propeller and the resulting propulsive performance of the ship. This study provides a straightforward approach for gaining insight into how hull design can influence the performance of ships in waves.

KEY WORDS: CFD; Fixed hull; Waves; Performance; Boundary layer; Propeller inflow

INTRODUCTION

The reliability of performance predictions for ships when subjected to offshore conditions by means of CFD has been a topical subject in recent years. This comes from the fact that proper verification and validation of *numerical towing tank* techniques is not well established in many areas (Stern et al., 2006). Addressing this issue, recent CFD workshops based on benchmark test cases (Hino, 2005; Larsson et al., 2003, 2010) have shown encouraging results for the applicability of CFD to most aspects of ship performance. However, the lack of consistency and common problems areas have also been highlighted. One of the major issues that has been found is the inability to accurately predict the phase lag between the wave encounters and the resulting forces (Larsson et al., 2010)

One reason for this might be that a focus on correctly modelling the complex geometry (a ship moving in six degrees of freedom with a rotating propeller) has somewhat taken over from correctly modelling and understanding the important phenomena involved. Even though the moving geometry is what influences the performance the most, anyone looking to subtly improve the design of a hull to achieve a small percentage of increased efficiency must be able to quantify which factors are most influential. For example, a moving mesh technique may not be suitable to capture highly non-linear phenomena in the bow area resulting in a lag of the force distribution further aft. Furthermore, it has been shown that the flow situation at the bow influences the character of the boundary layer further aft (Landweber and Patel, 1979) but no qualitative study exist on what influence the surrounding seastate has on this interaction.

The flow around the hull, the character of the boundary layer and the inflow to the propeller ultimately act together to influence the overall performance of the ship in waves. Adding knowledge about how these interact differently because of differences in bow shape will provide a new insight into how important the correct modelling of the bow flow is.

APPROACH

The approach taken here is to study the influence of incoming waves on a series of fixed hulls with identical underwater shapes but different above water bow sections. This is done to demonstrate that even a change of the above water shape in moderate waves can have a significant enough effect on the boundary layer and on the flow around the hull to show up in the propeller plane. The propeller plane is chosen as a point of comparison because it allows both for studies of how the flow has been affected around the hull but also how this might affect propeller performance. The flow is modelled using RANS with the open source CFD package OpenFOAM. The setup of the numerical towing tank used has previously been validated against experiments by Windén et al. (2012). A Blade Element Momentum (BEM) modelling technique by Phillips et al. (2009, 2010) is used to model the propeller.

The Wigley hull is chosen as a base hull because of its simplicity. This will make it easier to distinguish what effects come from the changed bow shape and allow disturbances to travel downstream relatively easily. The negative aspect of this choice is that it makes the results less representative for what would be experienced with a realistic hullform. However, because the initial aim is to study the importance of what happens at the bow and to

identify what flow features gets influenced by this, the Wigley hull is seen as the most attractive option.

Six different bow sections with different flare angles are created from the base hull where one is the base hull itself with no flare for reference.

RANS MODELLING

The problem is modelled using the PISO algorithm (Issa, 1986) for pressure-velocity coupling with a Volume of Fluid (VOF) approach for capturing the effects of the free surface. Turbulence is modelled using the $k-\omega$ SST model by Menter et al. (2003).

Geometry

The setup of the numerical towing tank is shown in Figure 1. Waves are generated and dissipated using the relaxation-based wave generation toolbox waves2Foam (Jacobsen et al., 2012). The length of the relaxation zones are chosen to be twice the wavelength so that $L_g = L_d = 2\lambda$. The size of the computational domain is set so that $L_F = L$ and $L_a = 4L$. Forward speed is modelled using a steady current which is set corresponding to $Fn = 0.2$. The waves are chosen to have an amplitude of $\zeta = 0.023m$ which corresponds to about 12% of the model draught. The wavelength is set to be equal to the model length so that $\lambda = L$.

The particulars of the chosen hull are shown in Table 1. These remain unchanged for all six hulls since the modification only concerns the above water shape.

Table 1: Particulars of tested hulls

L	3 m	B	0.3 m	a_2	0.2
T	0.1875 m	∇	0.0780 m^2		

where a_2 gives the shape of the hull as

$$z = \frac{B}{2}\left[1-\left(\frac{y}{T}\right)^2\right]\left[1-\left(\frac{2x}{L}\right)^2\right]\left[1+a_2\left(\frac{2x}{L}\right)^2\right] \quad (1)$$

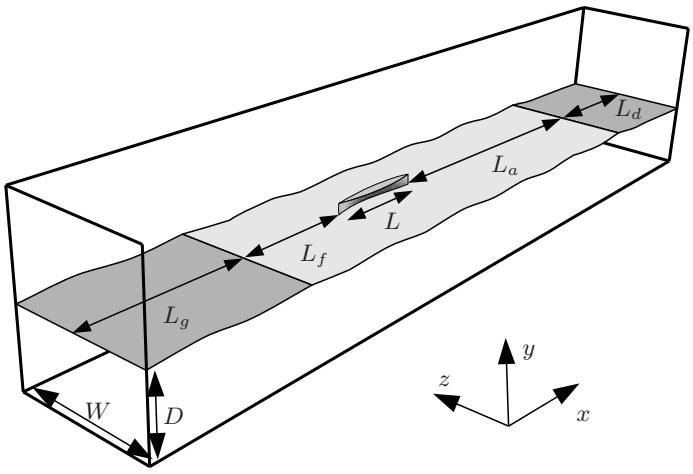

Figure 1: Geometry of the numerical towing tank

Meshing

The mesh is created using an automated algorithm described by Windén et al. (2012). The emphasis is to create smooth transitions between areas of different aspect ratios and cell sizes such as the free surface region, the wake region and the far field. The mesh density in the free surface region has a large impact on the quality of the propagating regular waves. Windén et al. (2012) found that, for this setup, 30 cells per waveheight and 30 cells per wavelength should be enough to ensure undisturbed propagation. The near wall spacing is set to a y^+-value of 50-60 for the hull and wall functions on k and ω are thus utilised. The mesh for the base hull with no flare is shown in Figure 2.

The mesh size varies slightly between the different cases but is around 12M cells. When considering RANS modelling of ships in waves as a practical design tool, this number is too high to be feasible. However, it is used here since quality rather than quantity and speed of results are considered more important. The extra cells are spent on a fine resolution at the bow, the wake and the boundary layer as well as ensuring that waves are resolved properly as explained earlier. Furthermore, the free surface resolution close to the hull is much higher than the 30 cells per waveheight/-length in the freestream. This is done to capture smaller waves and interaction between the hull generated waves and the incident waves.

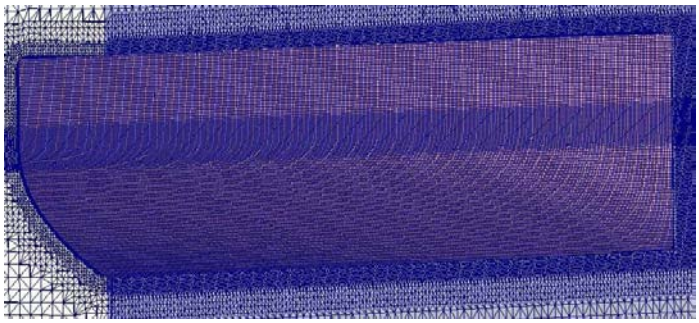

Figure 2: Mesh for base case showing the front half of the hull

FLARE SERIES

Flares on ship bows are usually associated with performance in waves in terms of damping of motions, slamming and deflection of very large waves. In this study the hull is locked and the waves are moderate. This is intentional since the aim is to show whether or not the bow shape can still influence the performance in more subtle ways and thus motivate more investigations into how the bow flow is resolved when using CFD. Both positive (outwards) and negative (tumblehome) flares are created to compare their effects. Tumblehome flares have recently been a topical means of improving performance in rough seas with the appearance of the Ulstein X-bow.

In this study a modified Wigley hull is used to represent the effects of different types of flare. The modified Wigley hull has the same definition of shape under the waterline as in Eqn. 1 but rather than being wall sided above the waterline, the hull is distorted to create a flare. If x_o, y_o and z_o are coordinates giving the shape of the original hull above the waterline, the modified hull is defined as:

$$x_m = \left\{ \begin{array}{llllll} x_o & if & x_o \geq x_\phi & or & y_o \leq 0 \\ x_o + \phi_x & if & x_o < x_\phi & \& & y_o > 0 \end{array} \right\} \quad (2)$$

$$z_m = \left\{ \begin{array}{llllll} z_o & if & x_{mo} \geq x_\phi & or & y_o \leq 0 \\ z_o \pm \phi_z & if & x_o < x_\phi & \& & y_o > 0 \end{array} \right\} \quad (3)$$

where

$$\phi_x = \phi_{amax} \left(\frac{y_o}{H}\right)^{n_x} \frac{(x_o - x_\phi)}{(0.5L + x_\phi)} \quad (4)$$

$$\phi_z = \left(\frac{B}{2} - |z_o|\right) \left(\frac{y_o}{H}\right)^{n_{z1}} \left(\frac{x_o + 0.5L}{x_\phi + 0.5L}\right)^{\frac{1}{n_{z2}}} \quad (5)$$

and with $y_m = y_o$. H is the freeboard, ϕ_{amax} the maximum overhang in the x direction, and x_ϕ the start of the flare region. The exponents n_x and n_{z1} determine the curvature of the flare. The exponent n_{z2} determines the curvature and extent of the deck. All parameters relating to the flare are defined in Figure 3.

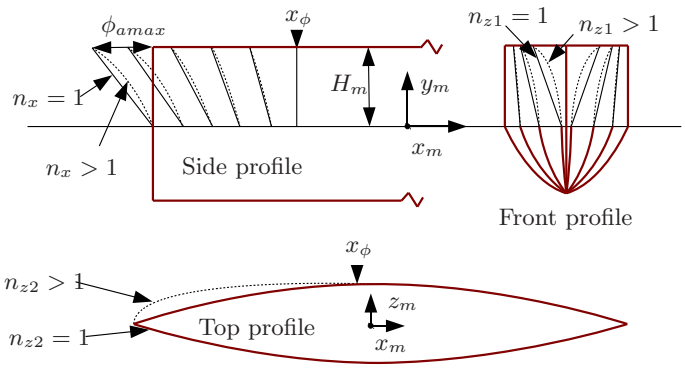

Figure 3: Definition of flare parameters on hull

Six hulls were tested. The parameters $n_x = n_{z1} = n_{z2} = 3$ and $x_\phi = 0$ were fixed and the overhang ϕ_{amax} was varied according to Table 2. Here Flare 4 is the reference hull with no flare. According to the definition in Figure 3, Flares 1-3 are tumblehome flares whereas Flares 5 and 6 are sloping outwards. The resulting six bow sections are shown in Figure 4.

Table 2: Description of flared hull series

Hull ID	ϕ_{amax}
Flare 1	-6.3 % of *Lpp*
Flare 2	-4.2 % of *Lpp*
Flare 3	-2.1 % of *Lpp*
Flare 4	0
Flare 5	2.1 % of *Lpp*
Flare 6	4.2 % of *Lpp*

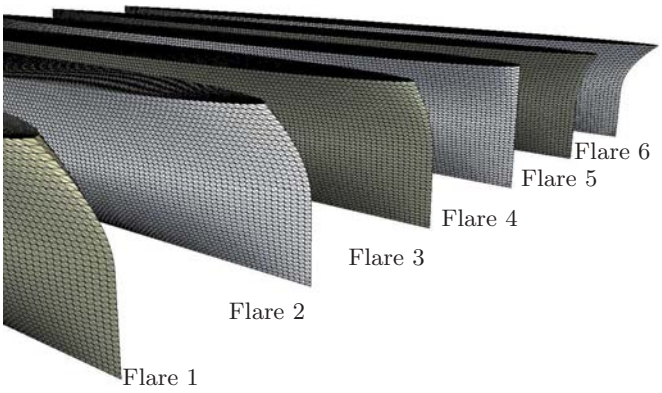

Figure 4: Visualisation of tested bow sections

For reference the calm water resistance R_{CW} and the added resistance in waves R_{AW} for the used hulls are shown in Figures 5 and 6. This study is focused mainly on the flow f

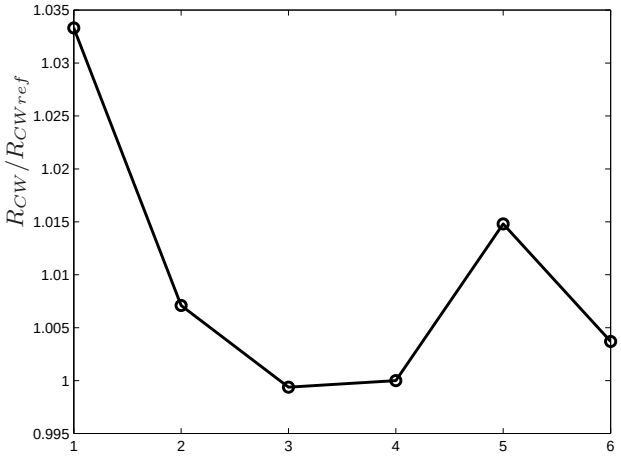

Figure 5: Calm water resistance for the tested bow sections

The added resistance in waves R_{AW}, defined here as the mean increase in resistance due to waves as

$$R_{AW} = mean(R_W(t)) - R_{CW} \quad (6)$$

where $R_W(t)$ is the measured resistance in waves over a period of time. R_{AW} is shown for the different bow shapes in Figure 6. Even though a large variation of R_{AW} is shown here, the absolute values are small at around 0.5-0.6% of R_{CW} for all bows. This is due to the fact that none of the usual main sources of added resistance, heaving, pitching and blunt bows are present here.

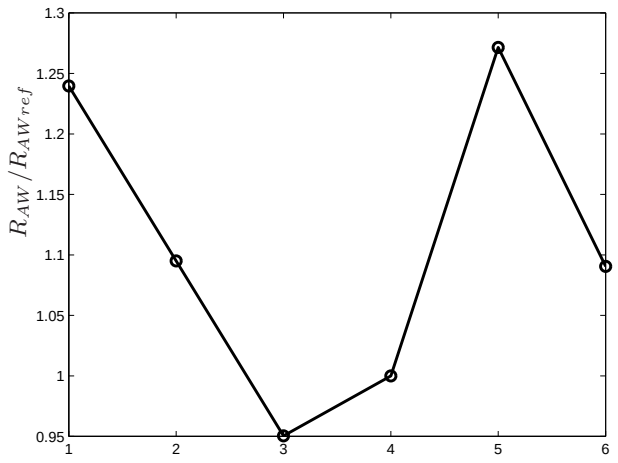

Figure 6: Added resistance in waves for the tested bow sections

PROPELLER PLANE ANALYSIS

The Wigley hull is a purely academical hullform and has no consideration of propeller positioning in the definition of its shape. The propeller disc is therefore positioned half a diameter behind the aft perpendicular, with a lower point flush with the keel and with a diameter of 85% of the draught. This is seen as representative of a typical positioning of the propeller on a ship. The positioning of the propeller disc relative to the rear profile of the used Wigley hull is shown in Figure 7.

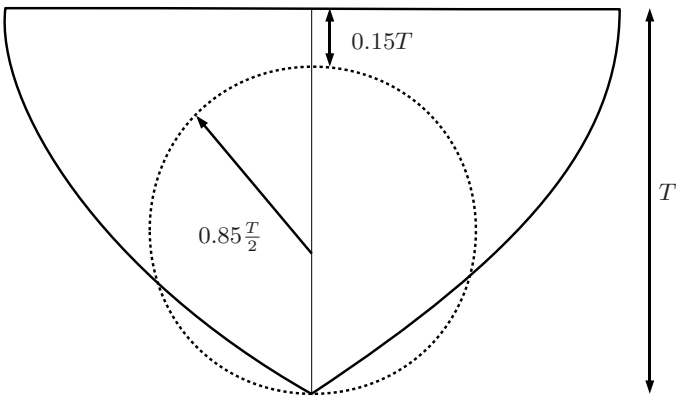

Figure 7: Positioning of propeller disc behind Wigley hull

Propeller Inflow Analysis

The flow field through the propeller disc, positioned as in Figure 7, is analysed. Velocities are probed in the propeller plane using a uniform spacing of points 0.0015m (1.9% of the propeller radius) apart. Results are presented here as the difference in the flow variables U_x and k, representing axial velocity and turbulence kinetic energy between the reference hull and hulls with different bow sections. The inflow profiles are averaged to represent mean conditions in waves. This is done over a series of wave periods with about 1000 samples for each encounter with the sample frequency being determined by the time step of the simulation. Between three and four encounter periods the total change in the average at all the points amounted to less than 0.5 %. Based on this, three periods was chosen as the averaging scope and the resulting average profiles are shown in in Figure 8.

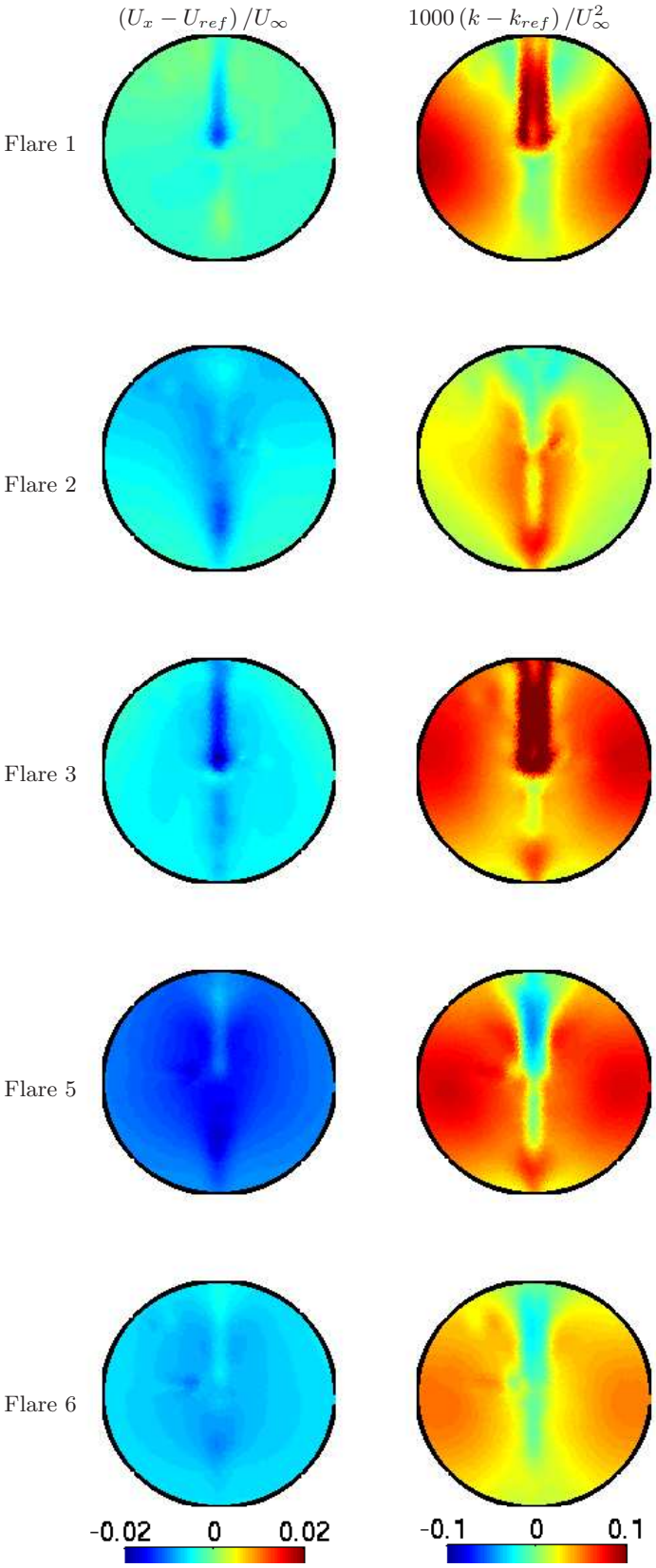

Figure 8: Difference from reference case in propeller inflow for different bow sections, averaged over $3T_e$

For reference, U_x and k for the reference case are also shown in Figure 9 where the remains of the turbulent boundary layer can

be seen as the two areas of high turbulence intensity on each side of the centreline in the upper part of the propeller disc. This is also the area where the most change is seen between different bows in Figure 8. This indicates that the way the boundary layer separates from the stern is different between the cases with a lower level of separation leading to an increase in intensity towards the centreline as shown for Flare 3 and 1 and vice versa for Flare 2,5 and 6. This is supported by a decrease in U_x towards the centreline for those flares with increased k and vice versa. A large increase of k is also seen centred at about $0.95R$, horizontally away from the propeller centre for all flares except Flare 2.

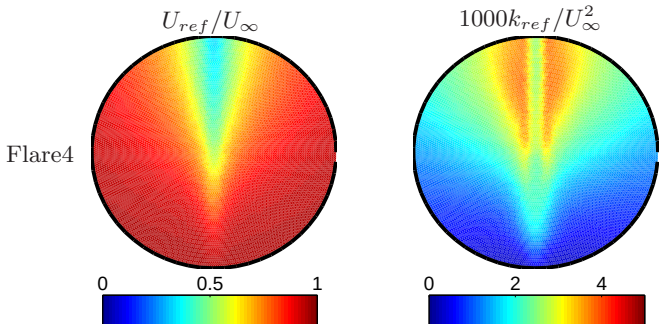

Figure 9: Axial velocity and turbulence intensity in the propeller plane for reference case, averaged over $3T_e$

In Figure 8, it can be seen that the average velocity going in to the propeller changes between 0 and ±2% of the free stream velocity depending on the bow shape. The largest difference from the reference case is seen for Flare 5 which is a moderate outwards flare.

A more significant effect of the bow shape change is seen in the turbulence kinetic energy k. A change of ±10% is seen both for the relative difference $1000\,(k - k_{ref})\,/U_\infty^2$ but also for the absolute ratio k/k_{ref} which is not shown here. Increased levels of turbulence can lead to both increased noise generation by the propeller as well as changes in the produced thrust (Morton, 2012). Studies on wind turbines show that different levels of atmospheric turbulence can change the power output for a turbine by up to 20% (Lundquist and Clifton, 2012). Even though the differences recorded here are unlikely to have an impact even close to that number, it still suggests that the bow flow has impacts on the overall performance reaching far beyond the pressure distribution at the bow itself.

Another effect of the turbulence in the propeller inflow is the effect it might have on the inception of cavitation. Korkut and Atlar (2002) showed that the free stream turbulence is contributing to complex scaling effects when predicting cavitation and that this is often neglected. It must be noted here that results regarding turbulence intensity must be seen with some scepticism for this case. The upper parts of the propeller plane are close to the free surface and the $k-\omega$ SST model, as well as any common turbulence model does not produce accurate results close to the interface when using a VOF method (Shirani et al., 2006).

BEM Analysis

To get an estimate how the changes in the inflow condition might affect a working propeller, the time dependant velocities are given as wake profiles to a BEM code developed by Phillips et al. (2009, 2010). By doing so, the time variation of thrust and torque coefficients KT and KQ as well as the propeller efficiency η can be found. The efficiency is defined as

$$\eta = \frac{Delivered\,power}{Shaft\,power} = \int_{Blade} \frac{J_{local} KT}{2\pi KQ} \tag{7}$$

where J_{local} is the local advance coefficient along the blade. The properties used for the propeller model are shown in Table 3.

Table 3: Properties used in BEM model

Property	Notation	Value used
Advance ratio	J	0.6
Pitch/Diameter ratio	P_D	0.73
Blade area ratio	B_R	0.58
Number of blades	N	4
Radius	R	$0.85T/2$

The velocities are probed at 10 different radii corresponding to 10,20,30,40,50,60,70,80,90 and 100% of the total radius R. The hub radius is assumed to be $0.2R$ and the torque and thrust contributions at the blade tip are assumed to be zero. Consequently the velocities at $0.1R$ and R are discarded in the calculation. For each radius, 50 circumferential sections are used in the calculation.

An example of the output KT from the BEM for Flare 3 is shown in Figure 10.

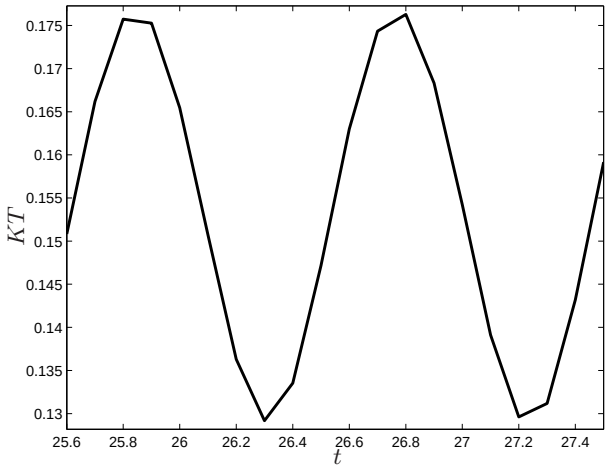

Figure 10: Variation of KT under waves for Flare 3

From the time variation of η, KT and KQ, mean values and oscillation amplitudes are extracted. The difference of these from the reference case are presented for all flares in Figure 11.

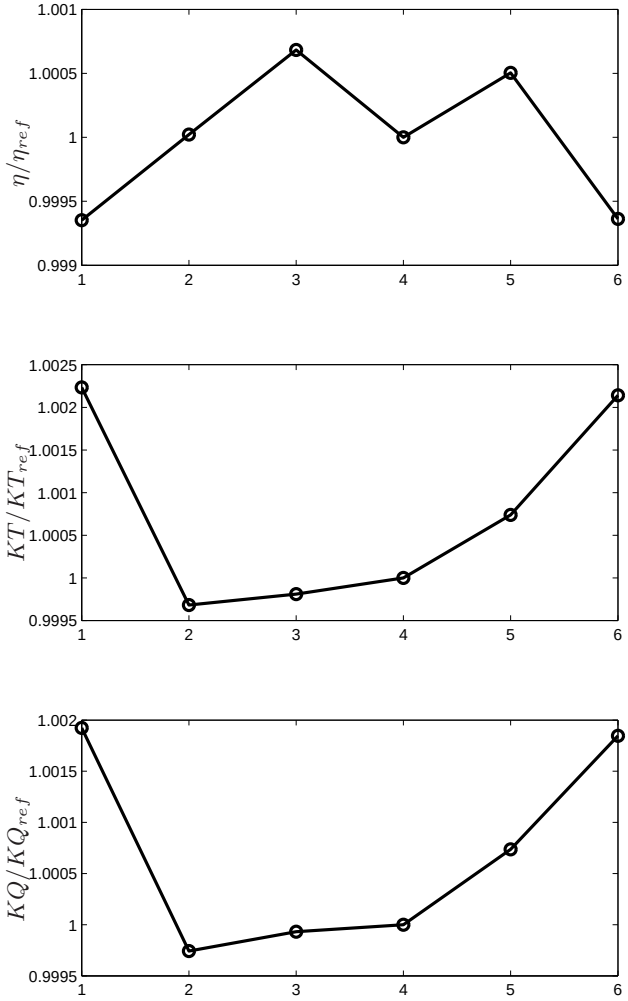

Figure 11: Difference in mean performance compared to reference case for different bow sections

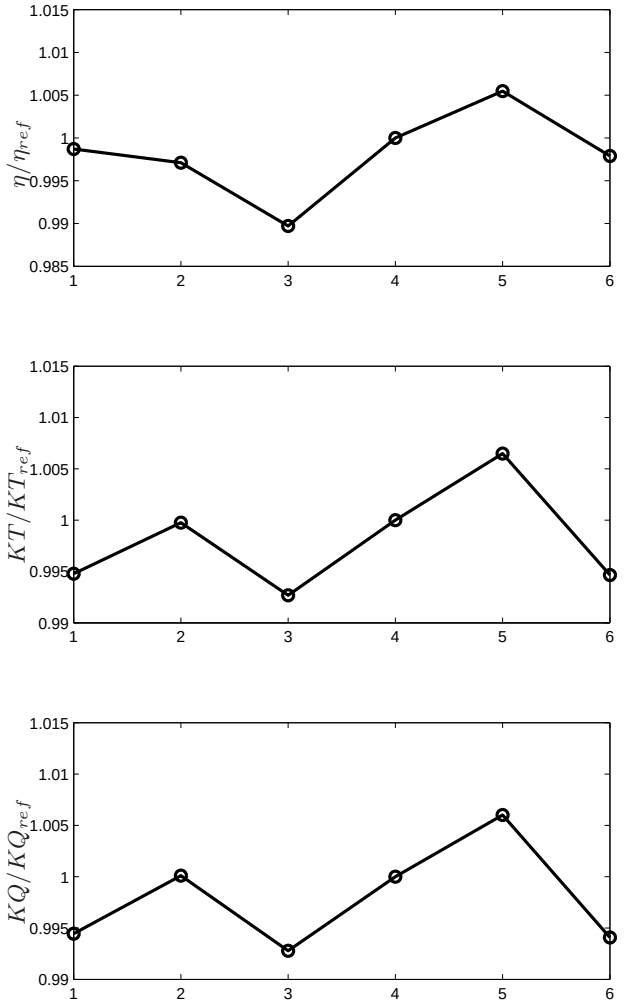

Figure 12: Difference in performance oscillation amplitude compared to reference case for different bow sections

It is evident that for a fixed hull in moderate waves, the influence of the bow shape on mean propeller performance is very small. The largest recorded thrust increase is is about 0.2%, a value that must be considered well within the error margins of both the RANS model and the BEM model, let alone both combined. A slightly more significant effect from the change of bow shape is seen when looking at the amplitude of the performance variations with time. This is shown in Figure 12 where a difference of $\pm 1\%$ from the reference case is demonstrated. Unsteady periodic loading of the propeller is usually associated with separation vortices behind complex sterns. However, in this case since the Wigley hull experiences very little separation, they stem from orbital velocities due to the passing waves.

Periodic oscillations of thrust and torque risks leading to fatigue problems in the propeller shafting and in the hull (Molland et al., 2011). Increased amplitudes of these oscillations may increase that risk and equally, decreased amplitude may mitigate it so propellers are usually designed to minimise these fluctuations (Molland et al., 2011).

The difference in the amplitude of oscillations and the mean flow velocity for different bow shapes may have several causes.

- Differences in how the regular wave pattern is disturbed by the passing ship.
- Differences in how oscillations created at the bow are carried aft in the boundary layer.
- Differences in how streamlines passing under the hull reemerge at the stern (caused by different initial trajectory at the bow.)

FLOW ANALYSIS

These causes are hard to quantify, analyse and visualise in a short and concise way so they will mostly be left as future work. The wave pattern however, can be quickly analysed to see if it has any influence in this case.

The profile of the bow wave at the time of a wave crest passing the forward perpendicular is extracted. The profiles for the two largest (negative and positive) flares are shown in Figure 13.

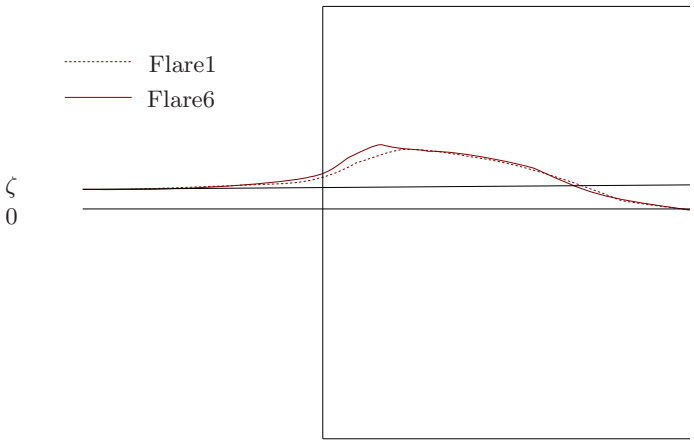

Figure 13: Bow wave profiles for the two largest flares

The profiles are shown relative to the still water level 0 and the amplitude of the regular waves ζ. The overall profile is relatively unchanged between the two bows but the outward flare produces a slightly steeper and higher bow wave. The difference in the maximum height is about 25% of the regular wave height ζ and 3% of the draught.

A similar analysis is made of the stern wave. This is extracted at the same point in time as the bow wave profiles and, since $\lambda = L$, is also shown at a passing of a wave crest. The rear profiles of the wave elevation at the aft perpendicular for the two different bows are shown in Figure 14.

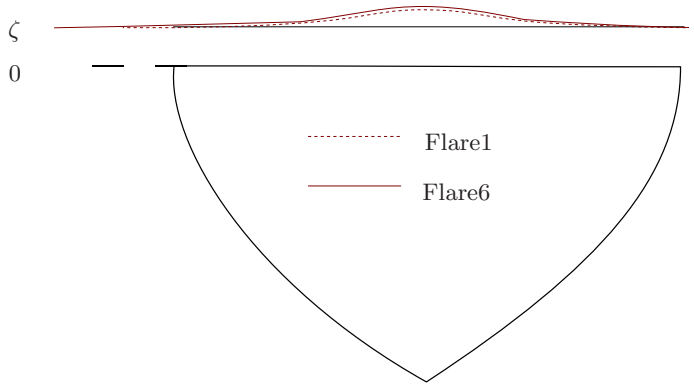

Figure 14: Stern wave profiles for the two largest flares

The difference in height of the stern waves between Flare1 and Flare6 is about 8% of the wave height ζ and 1% of the draught. Some of the effects of the different bow shape can thus still be seen at the stern. However, this is confined to a very small area, in a wave riding on top of the crest of the regular wave (i.e not affecting the propeller plane velocities shown in Figure 8.) The amplitude of the regular wave itself remains unchanged by the change in bow shape. The conclusion is thus that in this case, the wave pattern itself and its disturbance by the bow is not the cause of the differences in inflow velocities seen earlier.

CONCLUSIONS

A set of Wigley hulls with different above water bow shapes subjected to regular waves have been simulated in a numerical towing tank. The resulting propeller plane flow situation has been studied and propeller performance has been evaluated using a BEM. Furthermore some discussion has been shown around the behaviour of the wave pattern and how this might affect said performance.

The effect of the bow shape is mostly noticeable in two ways. It changes the amplitude of the periodic variations of thrust and torque with up to 1%. It also changes the intensity of the turbulence in the propeller inflow. Both of these factors have implications for noise generation as well as fatigue damages to the hull and propeller through vibrations and cavitation.

No decisive conclusion can be made as to which one of the bows tested performed best. Flare 3 shows the lowest added resistance, a decrease in the calm water resistance and a decrease in periodic thrust and torque variations. However, Flare 3 also showed the highest increase in the turbulence intensity experienced by the propeller. Not surprisingly, Flare6 shows the worst performance in most areas except for having the lowest increase in turbulence intensity in the propeller plane. Generally it seems that a moderate flare in any direction or indeed no flare is showing the best performance across the board. Flare 5 deviates from many of the trends shown in this study and it cannot be excluded that this is due to some error occurring in the simulation.

The study should not be seen as indicative of which bow shape is best to use for ships operating in rough weather. It should rather be seen as an indication that the flow at the bow has implications on the performance in many different ways. Future ship performance evaluations are likely to move more and more to CFD simulations and the margins of error and the percentage of improvements sought are likely to be getting ever lower. In light of this it is important to focus efforts not only on representing the complex geometry correctly, but also on capturing some of the phenomena discussed in this paper.

This study will be further extended by fully coupling the BEM with the RANS solver to improve the accuracy of the propeller performance predictions. The implementation of body force methods in OpenFOAM is available through previous work by Turnock et al. (2010). The study will also be extended to make the hull free to surge something that is likely to affect both the bow flow, the boundary layer and the flow at the propeller plane. Furthermore, the variations of the phenomena discussed in this paper with varying wavelength should be a topic of future interest. The added resistance in waves is highly dependent on wavelength and there will inevitably be different phenomena present for very short and very long waves that alters the situation shown in this paper.

ACKNOWLEDGEMENTS

All RANS-CFD simulations conducted as a part of this paper uses the open source CFD package OpenFOAM. The research has been conducted within the framework of the research project entitled *ship design for enhanced sustainability* which is sponsored by the Lloyd's Register Educational Trust who's support is gratefully acknowledged.

REFERENCES

Hino, T. (2005), CFD Workshop Tokyo 2005, Technical report.

Issa, R. (1986), 'Solution of implicitly discretized fluid flow equa-

tions by operator splitting', *Journal of Computational Physics* **62**, 40–65.

Jacobsen, N. G., Fuhrman, D. R. and Fredsøe, J. (2012), 'A Wave Generation Toolbox for the Open-Source CFD Library: OpenFoam©', *Int. J. Numerl. Meth. Fluids* **In print**.

Korkut, E. and Atlar, M. (2002), 'On the importance of the effect of turbulence in cavitation inception tests of marine propellers', *Proceedings of the Royal Society* **458**.

Landweber, L. and Patel, V. (1979), 'Ship Boundary Layers', *Annual Review of Fluid Mechanics* **11**, 173–205.

Larsson, L., Stern, F. and Bertram, V. (2003), 'Benchmarking of computational fluid dynamics for ship flows: the Gothenburg 2000 workshop', *Journal of Ship Research* **47**(1), 63–81.

Larsson, L., Stern, F. and Visonneau, M. (2010), Gothenburg 2010, A Workshop on Numerical Ship Hydrodynamics, Technical report.

Lundquist, J. and Clifton, A. (2012), 'How turbulence can impact power performance', *North American Wind Power* **9**(8).

Menter, F., Kuntz, M. and Langtry, R. (2003), Ten Years of Industrial Experience with the SST Turbulence Model, *in* 'Proceedings of the 4th International Symposium on Turbulence, Heat and Mass Transfer', pp. 625–632.

Molland, A., Turnock, S. and Hudson, D. (2011), *Ship Resistance and Propulsion: Practical Estimation of Ship Propulsive Power*, Cambridge University Press.

Morton, M. (2012), Rotor Inflow Noise Caused by a Boundary Layer: Inflow Measurements and Noise Predictions, M.sc. thesis, Virginia Polytechnic Institute and State University.

Phillips, A., Turnock, S. and Furlong, M. (2009), 'Evaluation of manoeuvring coefficients of a self-propelled ship using a blade element momentum propeller model coupled to a Reynolds averaged Navier Stokes flow solver.', *Ocean Engineering* **36**(15-16), 1217–1225.

Phillips, A., Turnock, S. and Furlong, M. (2010), 'Accurate capture of rudder-propeller interaction using a coupled blade element momentum-RANS approach.', *Ship Technology Research (Schiffstechnik)* **57**(2), 128–139.

Shirani, E., Jafari, A. and Ashgriz, N. (2006), 'Turbulence Models for Flows with Free Surfaces and Interfaces', *AIAA Journal* **44**(7).

Stern, F., Wilson, R. and Shao, J. (2006), 'Quantitative V&V of CFD simulations and certification of CFD codes', *International Journal for Numerical Methods in Fluids* **50**, 1335–1355.

Turnock, S., Lewis, S., Philips, A., Banks, J., Windén, B., Hudson, D. and Molland, A. (2010), Evaluating the self-propulsion of a container ship in a seastate using computational fluid dynamics, *in* 'William Froude Conference: Advances in Theoretical and Applied Hydrodynamics - Past and Future', p. 12.

Windén, B., Turnock, S. and Hudson, D. (2012), Validating Force Calculations using OpenFOAM© on a Fixed Wigley Hull in Waves, *in* 'Proceedings of the 15th Numerical Towing Tank Symposium, 7-9 October, Cortona, Italy', pp. 170–175.